Supplementary Material for Decomposition in Decision and Objective Space for Multi-Modal Multi-Objective Optimization

Monalisa Pal[a], Sanghamitra Bandyopadhyay[a,*]

[a]*Machine Intelligence Unit, Indian Statistical Institute, 203, Barrackpore Trunk Road, Kolkata - 700108*

Abstract

This is the supplementary material to demonstrate various concepts and experiments for performance analysis of the evolutionary frameworks proposed in "Decomposition in Decision and Objective Space for Multi-Modal Multi-Objective Optimization".

1. Introduction

This is a supplementary document for the article proposing graph Laplacian based Optimization using Reference vector assisted Decomposition (LORD) for Multi-Modal Multi-objective Optimization Problems (MMMOPs) [1] and its extension (LORD-II) for multi-modal many-objective optimization problems. This material is to assist the readers to obtain a deeper insight on various topics associated with the proposed approach. Kindly note that this is not a stand-alone document and bears reference to the main article proposing LORD and LORD-II.

This material consists of the following topics in its different sections:

1. Section 2 of this material describes the various performance indicators used to analyze the performance of LORD and LORD-II in the proposed work.
2. Section 3 provides the Cartesian coordinate plots of the Pareto-optimal sets (PSs) and the Pareto-fronts (PFs) of the 22 test instances of CEC 2019 test suite [2] and compares them with those obtained by MO_Ring_PSO_SCD (a state-of-the-art algorithm for MMMOPs) [3] and LORD (or LORD-II).
3. Section 4 of this material analyzes the diversity attainment behavior of LORD in both objective space and decision space.
4. Section 5 compares the outcome using kmeans clustering with spectral clustering to establish the benefit of the latter.
5. To provide an idea of the computational burden of the proposed algorithms, Section 6 presents an analysis.
6. Finally, the material is concluded in Section 7.

2. Brief Description of Performance Indicators

This section briefly describes the various performance indicators used to analyze the performance of LORD and LORD-II in the proposed work.

*Corresponding author

Email addresses: monalisap90@gmail.com (Monalisa Pal), sanghami@isical.ac.in (Sanghamitra Bandyopadhyay)

2.1. Convergence Metric

Convergence Metric [4, 5] (also known as generational distance [6]) indicates the convergence of the solutions in the estimated Pareto-optimal surface to the true Pareto-optimal surface. Let $\mathcal{A}$ be a non-dominated set of solutions and $\mathcal{H}_{CM}$ be a set of several points are sampled uniformly across the Pareto-optimal surface. Convergence metric (CM) is estimated by (1) as the sample mean of the minimum Euclidean distance $D_E(.)$ of the objective vectors estimating the Pareto-Front ($\mathcal{A}_{\mathbf{F}} = \{\mathbf{F}(\mathbf{X}_i)|\mathbf{X}_i \in \mathcal{A}\}$) from the points in the reference set ($\mathbf{H}_j \in \mathcal{H}_{CM}$), over the number of solutions in the approximated Pareto-Front. If CM is evaluated in the decision space $\mathcal{H}_{CM}$ is a representation of the true Pareto-optimal Set and instead of $\mathbf{F}(\mathbf{X}_i) \in \mathcal{A}_{\mathbf{F}}$, $\mathbf{X}_i \in \mathcal{A}$ is considered in (1).

$$CM(\mathcal{A}_{\mathbf{F}}, \mathcal{H}_{CM}) = \frac{1}{|\mathcal{A}_{\mathbf{F}}|} \sum_{i=1}^{|\mathcal{A}_{\mathbf{F}}|} \left(\min_{j=1}^{|\mathcal{H}_{CM}|} \left(D_E \left(\mathbf{F}\left(\mathbf{X}_i\right), \mathbf{H}_j \right) \right) \right), \quad \text{where } \mathbf{F}\left(\mathbf{X}_i\right) \in \mathcal{A}_{\mathbf{F}} \text{ and } \mathbf{H}_j \in \mathcal{H}_{CM} \tag{1}$$

2.2. Inverted Generational Distance

Inverted Generational Distance (IGD) [7, 8] gives an indication of the convergence as well as the diversity of the approximated Pareto-Front. Let $\mathcal{A}$ be a non-dominated set of solutions and $\mathcal{A}_{\mathbf{F}} = \{\mathbf{F}(\mathbf{X}_i)|\mathbf{X}_i \in \mathcal{A}\}$ be the estimated Pareto-Front. Similar to the evaluation of CM, IGD also requires a set $\mathcal{H}_{IGD}$ of N_{IGD} points sampled uniformly over the true Pareto-Front (if evaluated in the objective space). IGD is estimated by (2) as the sample mean of the minimum Euclidean distance $D_E(.)$ of the points in the reference set ($\mathbf{H}_j \in \mathcal{H}_{IGD}$) from the objective vectors constituting the approximated Pareto-Front ($\mathbf{F}(\mathbf{X}_i) \in \mathcal{A}_{\mathbf{F}}$), over the number of solutions in $\mathcal{H}_{IGD}$. If IGD is evaluated in the decision space $\mathcal{H}_{IGD}$ is a representation of the true Pareto-optimal Set and instead of $\mathbf{F}(\mathbf{X}_i) \in \mathcal{A}_{\mathbf{F}}$, $\mathbf{X}_i \in \mathcal{A}$ is considered in (2). In this work, IGDF is used to represent IGD in objective space and IGDX is used to represent IGD in decision space.

$$IGD(\mathcal{A}_{\mathbf{F}}, \mathcal{H}_{IGD}) = \frac{1}{|\mathcal{H}_{IGD}|} \sum_{j=1}^{|\mathcal{H}_{IGD}|} \left(\min_{i=1}^{|\mathcal{A}_{\mathbf{F}}|} \left(D_E \left(\mathbf{F}\left(\mathbf{X}_i\right), \mathbf{H}_j \right) \right) \right), \quad \text{where } \mathbf{F}\left(\mathbf{X}_i\right) \in \mathcal{A}_{\mathbf{F}} \text{ and } \mathbf{H}_j \in \mathcal{H}_{IGD} \tag{2}$$

2.3. Hypervolume Indicator

Hypervolume Indicator [4, 9] can also represent both convergence and diversity information using a single value and also its evaluation is independent of the knowledge of the true Pareto-Front. For its evaluation, a hyper-rectangle is considered between a reference point ($\mathbf{R}_{HV}$) and the origin of the objective space. A set of points (say $\mathcal{H}_{HV}$) is randomly sampled in this hyper-rectangle using Monte-Carlo simulation. Hypervolume Indicator (HV) is given by (3) which yields the fraction of the points in $\mathcal{H}_{HV}$ which are Pareto-dominated by the non-dominated set of solutions, approximating the Pareto-Front (denoted by $\mathcal{A}_{\mathbf{F}}$). For its evaluation, an attainment function ($\alpha_{HV}(.)$) is defined which returns 1 when a point $\mathbf{H}_j \in \mathcal{H}_{HV}$ is dominated by any solution ($\mathbf{F}\left(\mathbf{X}_i\right) \in \mathcal{A}_{\mathbf{F}}$). Hypervolume Indicator is given by the average of the values returned by the attainment function over the set of points belonging to $\mathcal{H}_{HV}$.

$$HV\left(\mathcal{A}_{\mathbf{F}}, \mathcal{H}_{HV}\right) = \frac{1}{|\mathcal{H}_{HV}|} \sum_{j=1}^{|\mathcal{H}_{HV}|} \alpha_{HV}\left(\mathbf{H}_j, \mathcal{A}_{\mathbf{F}}\right), \quad \text{where } \mathbf{H}_j \in \mathcal{H}_{HV} \text{ and } \alpha_{HV}\left(\mathbf{H}_j, \mathcal{A}_{\mathbf{F}}\right) = \begin{cases} 1, & \text{if } \exists \mathbf{F}\left(\mathbf{X}_i\right) \in \mathcal{A}_{\mathbf{F}} \text{ with } \mathbf{F}\left(\mathbf{X}_i\right) \prec \mathbf{H}_j \\ 0, & \text{otherwise} \end{cases} \tag{3}$$

2.4. Pareto-Set Proximity

Pareto-Set Proximity (PSP) [3] is used to evaluate the similarity between the approximated Pareto-optimal Set ($\mathcal{A}$) and the true Pareto-optimal Set (represented by a set $\mathcal{H}_{IGD}$ of N_{IGD} points sampled uniformly on the true Pareto-optimal Set). PSP is given by (4) where *cov_rate* represents the cover rate (overlap ratio of the approximated Pareto-optimal Set to the true Pareto-optimal Set) and $IGD\left(\mathcal{A}, \mathcal{H}_{IGD}\right)$ represents IGDX. In (4), x_i^{min} and x_i^{max} represent the minimum and maximum along the i^{th} decision variable over the approximated Pareto-optimal Set, respectively. Similarly, x_i^{MIN} and x_i^{MAX} represent the minimum and maximum along the i^{th} decision variable over the true Pareto-optimal Set[1], respectively. While *cov_rate* indicates overlap, $IGD\left(\mathcal{A}, \mathcal{H}_{IGD}\right)$ represents convergence and diversity of the approximated Pareto-optimal Set with respect to true Pareto-optimal Set. Thus, PSP quantifies an overall quality of the approximated Pareto-optimal Set.

$$
\begin{aligned}
PSP\left(\mathcal{A}, \mathcal{H}_{IGD}\right) &= \frac{cov\_rate}{IGD\left(\mathcal{A}, \mathcal{H}_{IGD}\right)} \\
\text{where } cov\_rate &= \left(\prod_{i=1}^{N} \gamma_i\right)^{\frac{1}{2N}}, \\
\gamma_i &= \begin{cases} 1, & \text{if } x_i^{MAX} = x_i^{MIN} \\ 0, & \text{if } x_i^{min} \geq x_i^{MAX} \vee x_i^{max} \leq x_i^{MIN} \\ z_i, & \text{otherwise} \end{cases} \\
\text{and } z_i &= \left(\frac{min(x_i^{max}, x_i^{MAX}) - max(x_i^{min}, x_i^{MIN})}{x_i^{MAX} - x_i^{MIN}}\right)^2
\end{aligned}
\tag{4}
$$

2.5. Diversity indicator: D_metric

This indicator is a measure of the diversity of the population in the objective space [10]. Let S_k^G represent the number of objective vectors associated with the k^{th} reference vector at generation G. Ideal value of $S_k^G = S_{ideal}^G = n_{pop}/n_{dir}$ where n_{pop} is the size of the population and n_{dir} is the number of reference vectors. At generation G, D_metric^G is defined by (5) which has an ideal value of zero implying best diversity. A higher value of *D_metric* implies poor diversity. Thus, *D_metric* of the population at termination of an EA is gives the diversity attained by the estimated Pareto-Front [10].

$$
D\_metric^G = \frac{n_{dir}}{n_{pop}} \sqrt{\sum_{k=1}^{n_{dir}} (S_k^G - S_{ideal}^G)^2} \tag{5}
$$

2.6. Non-Contributing Solutions and Associated Indicators

As seen from (2), IGDX evaluation involves the term $\min\limits_{\mathbf{X}_i \in \mathcal{A}} \left(D_E\left(\mathbf{X}_i, \mathbf{H}_j\right)\right)$ where $\mathbf{H}_j \in \mathcal{H}_{IGD}$. A solution $\mathbf{X}_i^{NS} \in \mathcal{A}$ is called a non-contributing solution, if for a given representation of the true Pareto-optimal Set ($\mathcal{H}_{IGD}$) and a given set of non-dominated solutions ($\mathcal{A}$) the condition in (6) is satisfied [6, 11].

$$
\nexists \mathbf{H}_j \in \mathcal{H}_{IGD} : D_E\left(\mathbf{X}_i^{NS}, \mathbf{H}_j\right) = \min_{\mathbf{X}_i \in \mathcal{A}} \left(D_E\left(\mathbf{X}_i, \mathbf{H}_j\right)\right) \tag{6}
$$

Let the subset of the non-dominated solution set consisting of all such non-contributing solutions be $\mathcal{A}^{NS}$. The proportion of non-contributing solutions in the non-dominated solution set is given by $NSX = \left|\mathcal{A}^{NS}\right| / |\mathcal{A}|$. In this work, this proportion NSX is reported as an indicator to reflect the amount of outliers i.e., how many non-dominated solutions of the final population are not the nearest neighbors of any point in $\mathcal{H}_{IGD}$ (the set representing the true Pareto-optimal Set).

[1]It should be noted x_i^{MIN} and x_i^{MAX} are the bounds of the i^{th} variable over true Pareto-optimal Set, not over the decision space $\mathcal{D}$.

Table 1: Cartesian coordinate plots of PSs and PFs for some 2-objective MMMOPs viz. MMF1 to MMF7 and MMF1_z and MMF1_e.

	Pareto-optimal Set (PS)			Pareto-Front (PF)		
	True	LORD	MO_Ring_PSO_SCD	True	LORD	MO_Ring_PSO_SCD
MMF1	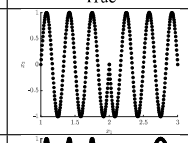	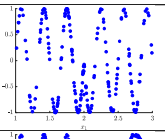	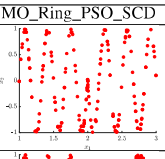	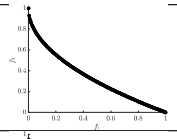	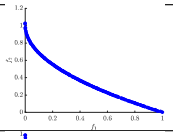	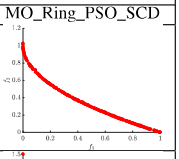
MMF1_z	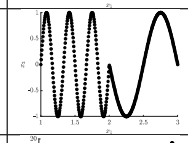	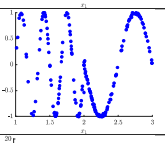	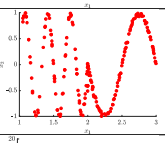	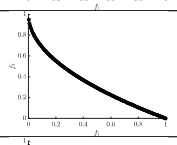	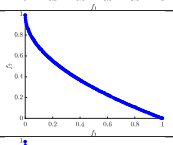	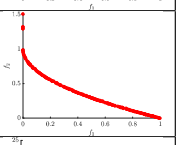
MMF1_e	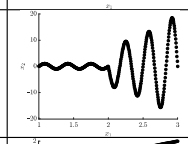	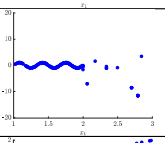	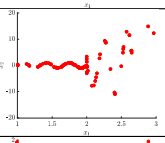	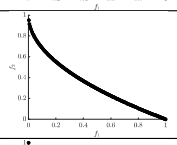	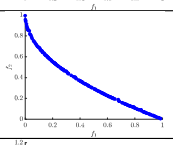	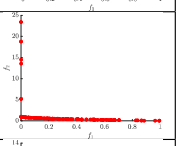
MMF2	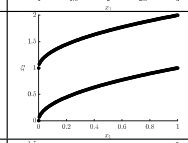	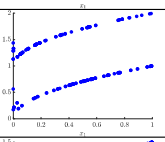	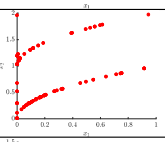	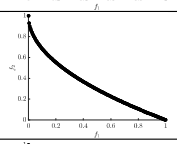	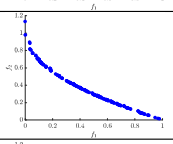	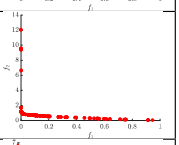
MMF3	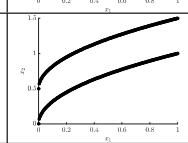	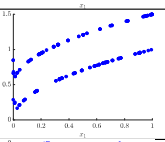	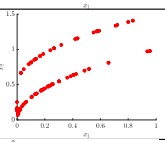	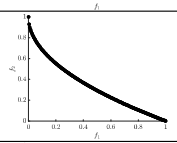	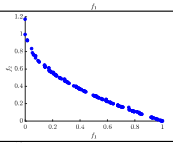	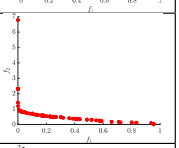
MMF4	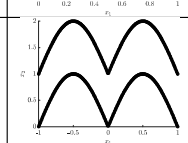	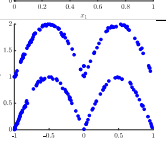	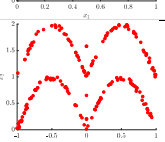	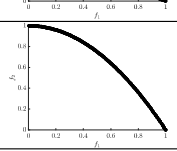	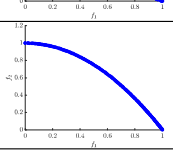	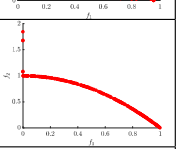
MMF5	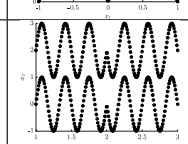	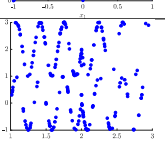	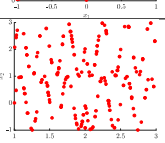	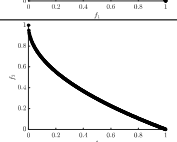		
MMF6						
MMF7						

Removing $\mathcal{A}^{NS}$ from $\mathcal{A}$ does not change IGDX i.e., $IGD(\mathcal{A}, \mathcal{H}_{IGD}) = IGD(\mathcal{A} - \mathcal{A}^{NS}, \mathcal{H}_{IGD})$. However, to note how far the outliers are from the surface of true Pareto-optimal Set, in this work, the convergence metric of $\mathcal{A}^{NS}$ is evaluated in the decision space with respect to $\mathcal{H}_{CM}$ i.e., $CM\_NSX = CM\left(\mathcal{A}^{NS}, \mathcal{H}_{CM}\right)$. If both NSX and CM_NSX are large, it implies that a large number of solutions are far away from the true Pareto-optimal Set.

3. Comparison by Visualization of Results

The Cartesian coordinate plots of the 2-objective MMMOPs are presented in Tables 1 and 2. For comparison, the results of LORD, MO_Ring_PSO_SCD [3] and the ground truth (ideal solutions) are plotted.

Table 2: Cartesian coordinate plots of PSs and PFs for some 2-objective MMMOPs viz. MMF8 to MMF13 and Omni-test, SYM-PART simple and SYM-PART rotated.

	Pareto-optimal Set (PS)			Pareto-Front (PF)		
	True	LORD	MO_Ring_PSO_SCD	True	LORD	MO_Ring_PSO_SCD
MMF8	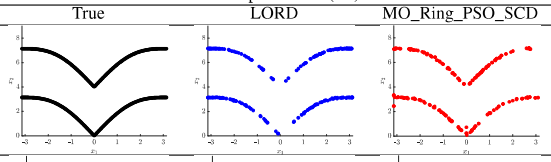			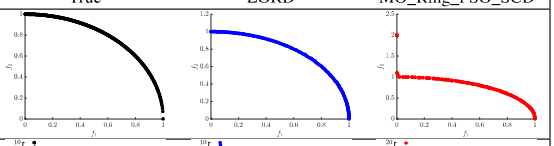		
MMF9	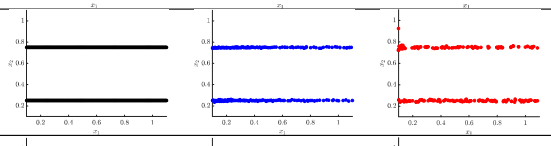			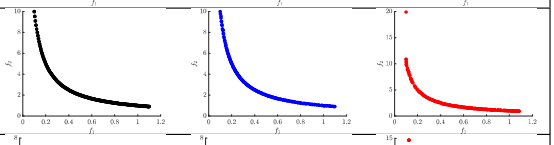		
MMF10	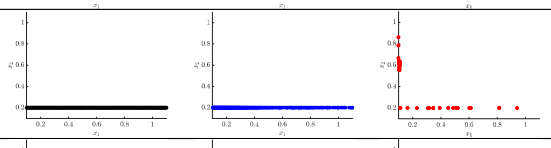			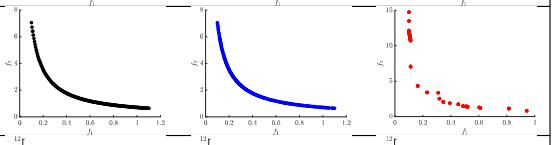		
MMF11	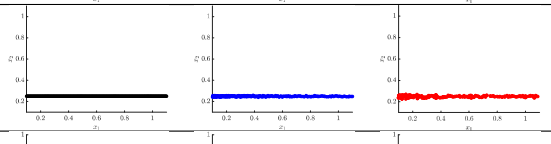			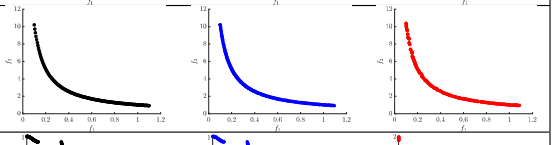		
MMF12	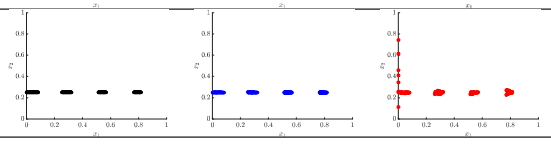			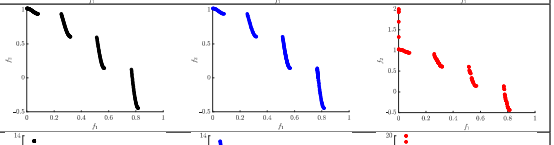		
MMF13	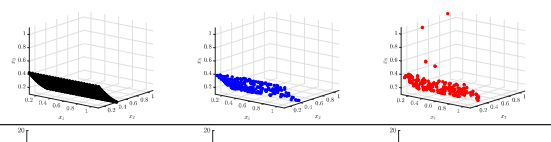			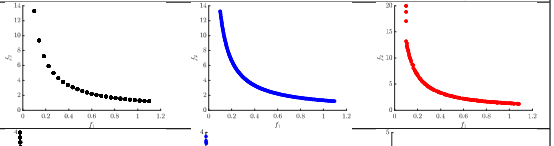		
SYM-PART simple	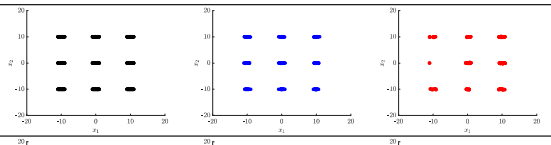			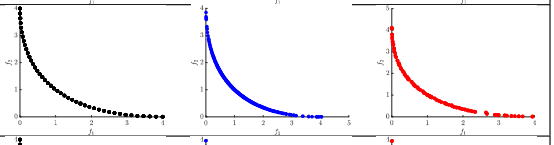		
SYM-PART rotated	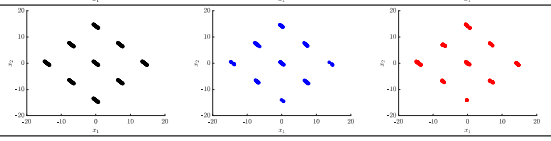			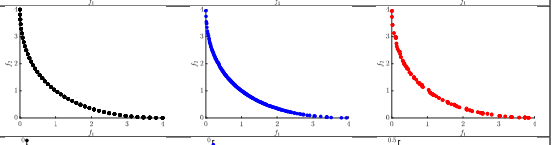		
Omni-test	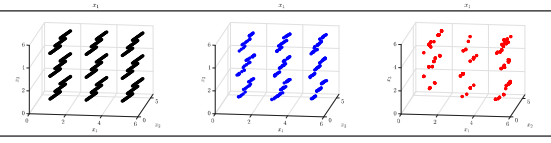			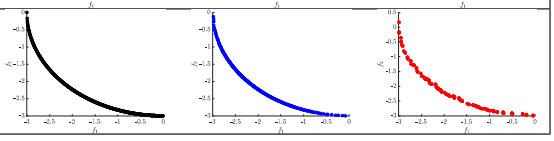		

Similarly, the Cartesian coordinate plots of the 3-objective MMMOPs are presented in Table 3 for comparing the results of LORD-II, MO_Ring_PSO_SCD [3] and the ground truth (ideal solutions).

3.1. Performance of LORD in objective space

It can be seen from Tables 1 and 2 that in most of the cases the number of outliers (points which have not converged on the ideal surface of PF) present in the results of MO_Ring_PSO_SCD are much more than those of LORD. This indicates the better convergence of LORD than MO_Ring_PSO_SCD. However, just on the basis of the plots, it is difficult to conclude regarding the diversity of solutions in the objective space as both the algorithms produce relatively uniform solution distribution.

Table 3: Cartesian coordinate plots of PSs and PFs for 3-objective MMMOPs.

	Pareto-optimal Set (PS)			Pareto-Front (PF)		
	True	LORD-II	MO_Ring_PSO_SCD	True	LORD-II	MO_Ring_PSO_SCD
MMF14(3)	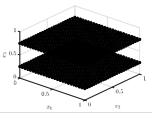	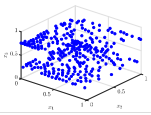	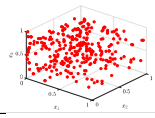	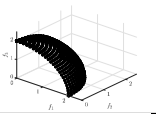	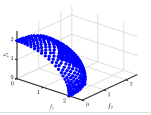	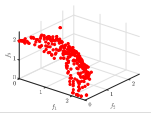
MMF14_a(3)	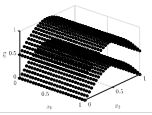	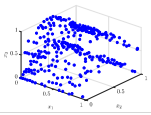	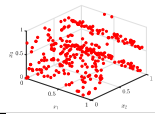	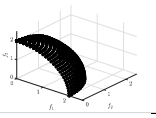	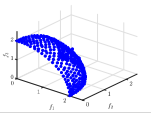	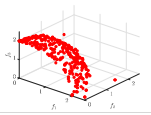
MMF15(3)	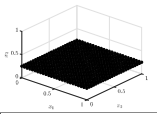	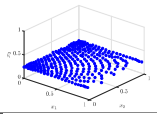	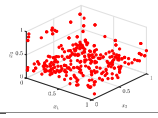	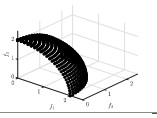	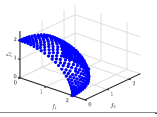	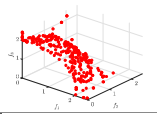
MMF15_a(3)	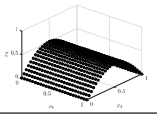	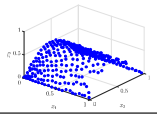	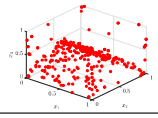	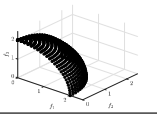	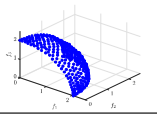	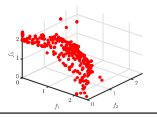

3.2. Performance of LORD in decision space

From Tables 1 and 2, it can be seen for all MMMOPs except MMF1_e and MMF8, the solution distribution in the decision space is atleast as good as that provided by MO_Ring_PSO_SCD. In some cases, such as MMF2, MMF3 and MMF10, the solution distribution is evidently superior than those obtained by MO_Ring_PSO_SCD. The poor performance for MMF1_e and MMF8 indicates the need for better decomposition methods in the decision space.

3.3. Performance of LORD-II in objective space

While MMF14 and MMF14_a are implemented to have one global PF, MMF15 and MMF15_a have one global and one local PF. The PFs for these problems are a spherical non-convex surface with the global being located at a radius of 2 and the local being located at a radius of 2.2, centering the origin of the objective space, in the first hyper-octant. As seen from Table 3, in the same function evaluation budget, almost all candidates have converged on the global surface of PF for LORD-II which is not the case for MO_Ring_PSO_SCD.

3.4. Performance of LORD-II in decision space

To realize the reason behind presence of outliers for MO_Ring_PSO_SCD, the corresponding decision space can be analyzed. While MMF14 and MMF14_a are implemented to have two global PSs, MMF15 and MMF15_a has one global and one local PS. As shown in the true solutions in Table 3, the top-most PS for MMF14 and MMF14_a acts as a local PS for MMF15 and MMF15_a, respectively.

By looking into the decision space, it can be realized that for MMF15 and MMF15_a, many solutions are stuck at the local optimal surface for MO_Ring_PSO_SCD which has been successfully overcome by LORD-II. This establishes the superiority of LORD-II over MO_Ring_PSO_SCD.

4. Population Dynamics in Decision and Objective Space

The experiment performed in [3], which studies and compares the convergence behavior of MO_Ring_PSO_SCD in the decision space, is repeated in this work for comparing the corresponding behavior of LORD and LORD-II with MO_Ring_PSO_SCD [3] and DN-NSGA-II [12]. For this experiment, the proportion of solutions in each of the four distinct regions of MMF4 (Fig. 1a) is calculated per generation. Ideally, for uniformly distributed solutions, these proportions should reach and saturate at 25%. For all the EAs, $n_{pop} = 800$ and

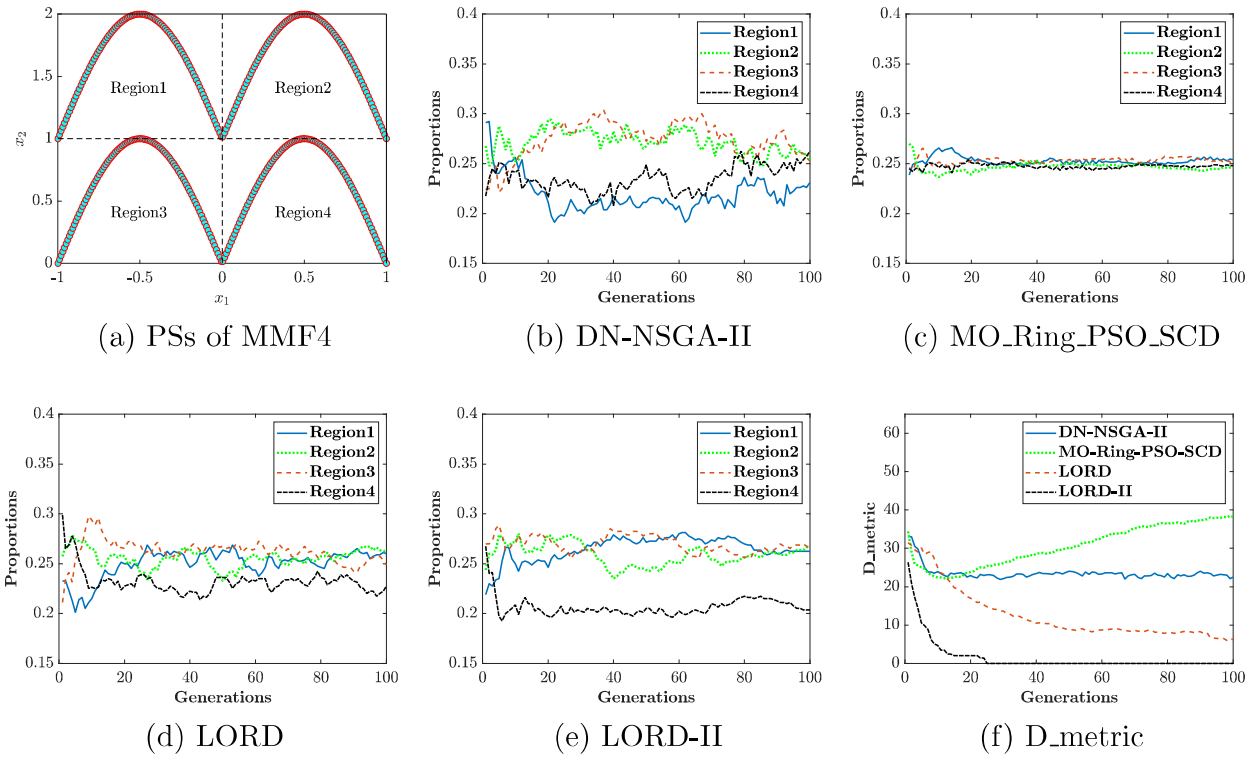

(a) PSs of MMF4 (b) DN-NSGA-II (c) MO_Ring_PSO_SCD

(d) LORD (e) LORD-II (f) D_metric

Figure 1: Solution distribution of MMF4 problem in the decision space (a), population dynamics in the decision space for four algorithms: DN-NSGA-II (b), MO_Ring_PSO_SCD (c), LORD (d) and LORD-II (e), population dynamics in the objective space using D_metric for these algorithms (f).

$G_{max} = 100$ is considered with the remaining parameters as specified in Section IV of the main manuscript. Each of the EAs are allowed to run 5 times and the mean proportions are plotted for DN-NSGA-II (Fig. 1b), MO_Ring_PSO_SCD (Fig. 1c), LORD (Fig. 1d) and LORD-II (Fig. 1e). As seen from these figures, the proportion of solutions in 3 regions is steady near 25-27% for both LORD and LORD-II. For LORD, the proportion in region 4 fluctuates between 20 to 25%, whereas for LORD-II, it is steady around 19-21%. Thus, the convergence behavior of LORD and LORD-II is intermediate between that of MO_Ring_PSO_SCD and DN-NSGA-II.

Along with the diversity of solution in decision space, the diversity of solution in objective space is also important. For this experiment, D_metric [10] is used as given by (5) with $n_{dir} = 800$. D_metric indicates the deviation between ideal and actual solution distribution in the objective space at the G^{th} generation and hence, it should be 0 ideally.

For the population at each generation, D_metric is obtained for all the four EAs and plotted in Fig. 1f. As shown, the diversity of solutions in objective space for MO_Ring_PSO_SCD severely deteriorates with generations. This may be a result of the crowding illusion described in Fig. 2 of the main manuscript. On the other hand, for LORD, although D_metric has not reached 0, a decreasing trend is observed. For LORD-II, the D_metric has reached the ideal value roughly by 25 generations. These evidences support the enhanced diversity preservation of the proposed frameworks in the objective space without sacrificing too much on the distribution in the decision space.

All the above-mentioned experiments establish the efficacy and the robustness of using the proposed LORD and LORD-II frameworks for addressing multi-objective optimization problems (MMMOPs or otherwise).

5. Spectral Clustering versus k-means Clustering

This experiment considers the example dataset in Fig. 1 of the main manuscript for MMF4 problem having four subsets in the PS. The outcome of clustering it using the approach outlined in Section 3.2 of the main manuscript is compared against the outcome of k-means clustering. For k-means clustering, $k = 4$ is used as MMF4 has 4 subsets in the PS. For spectral clustering, the thresholding factor α_L for the nearest neighbor graph was varied from 0.01 to 0.2 and best results were obtained for $\alpha_L = 0.046$. These results are illustrated in Fig. 2.

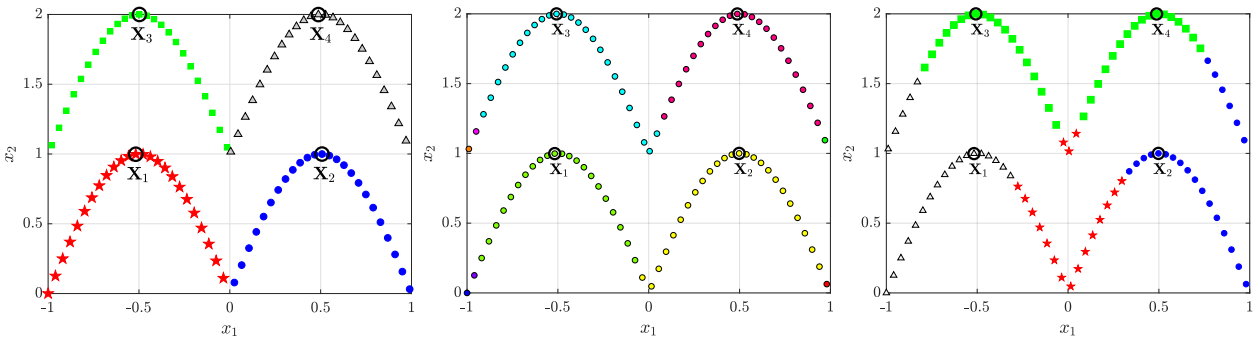

(a) True PS (Fig. 1a) (b) Spectral Clustering (proposed) (c) k-means Clustering

Figure 2: Comparing the outcome of spectral clustering with k-means clustering on MMF4 problem.

As seen from Fig. 2, the proposed method (using spectral clustering) can efficiently separate $\mathbf{X}_1$ to $\mathbf{X}_4$ into four different clusters. Specifically, it produces 10 clusters: 4 large clusters roughly corresponding to the 4 subsets in PS, and 6 singleton clusters in the boundary regions. On the other hand, each cluster produced by k-means spans over two or more subsets of the PS. Also, the four equivalent solutions $\mathbf{X}_1$ to $\mathbf{X}_4$ have not been separated into four distinct clusters using k-means. Thus, spectral clustering is more effective in dealing with the effects of crowding illusion.

6. Computational effort involved in filtering

The spectral clustering involved in the filtering stage involves the calculation of Euclidean distance between all pairs of candidates in a set of solutions $\mathcal{A}^{nd}$. Thus, the complexity of the filtering step involves a term $\mathcal{O}\left(\left|\mathcal{A}^{nd}\right|^2\right)$. This study is dedicated to show that in average case, this term doesn't have a large influence on the overall execution time of the proposed algorithms. The following points can be noted in this favor:

- Either of the filtering strategies (LORD/LORD-II) in the overall framework (Algorithm 1) is executed only if the parent candidate does not dominate the child candidate in line 7.
- As LORD and LORD-II are steady-state algorithms, this clustering may be done in an incremental/online manner [13] which can further reduce the complexity.
- Additionally, for LORD, the set $\mathcal{A}^{nd}$ to be clustered is only the last non-domination rank (R_c). It is expected that this set will be small in size towards early generations and gradually increase to population size (n_{pop}). Thus, an experiment is conducted to see the ratio of number of times the filtering is called with $\left|\mathcal{A}^{nd}\right|$ being within 10% of n_{pop} to $\left|\mathcal{A}^{nd}\right|$ being above 90% of n_{pop}. The average ratios are illustrated in Fig. 3. This experiment indicates that as almost all the ratios are above 1, 50% or more number of times clustering is called with $\left|\mathcal{A}^{nd}\right| \leq 10\%\ n_{pop}$.

Thus, the execution time of the entire algorithm is not very large. However, further research to improve the speed of the proposed algorithm is not the primary focus of the current work.

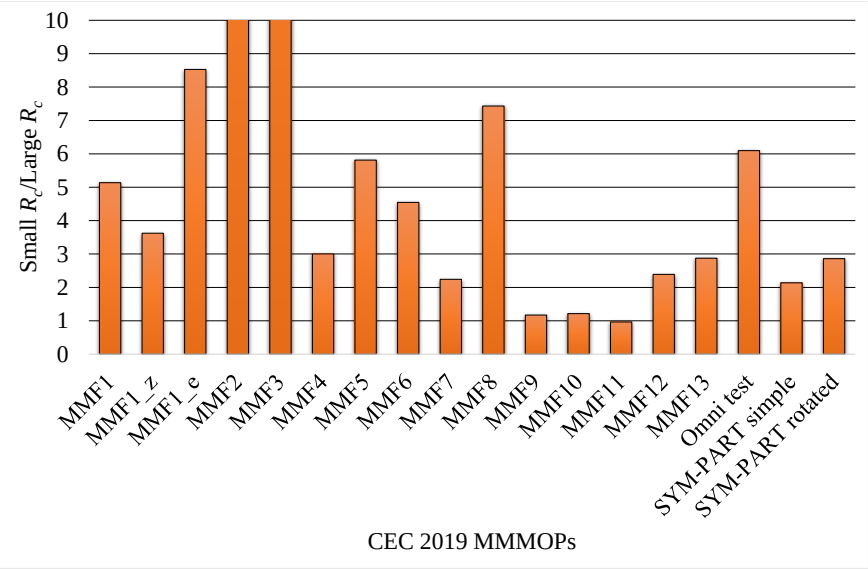

Figure 3: Ratio of number of filtering calls with $\left|\mathcal{A}^{nd}\right| \leq 10\%\ n_{pop}$ to $\left|\mathcal{A}^{nd}\right| \geq 90\%\ n_{pop}$. Note that this ratio is higher than 10 for MMF2 and MMF3.

7. Conclusion

As the modality of a real-world problem is often unknown, an evolutionary algorithm designed for MMMOPs, should also perform equally good for unimodal multi-objective optimization problems. Moreover, the convergence in the objective space is the foremost criteria to be established before dealing with the solution distributions in the objective and decision space. The proposed frameworks, LORD and LORD-II, provide themselves as robust alternatives for various kinds of multi-objective and many-objective optimization problems, respectively. Nonetheless, it is a preliminary work in this direction and better methods for improving the performance of evolutionary algorithms for MMMOPs are open for further research.

Acknowledgments

This work is partially supported by Indian Statistical Institute, Kolkata and by J. C. Bose Fellowship (SB/SJ/JCB-033/2016) of Department of Science and Technology, Government of India.

References

[1] R. Tanabe, H. Ishibuchi, A review of evolutionary multi-modal multi-objective optimization, IEEE Transactions on Evolutionary Computation (2019) 1–9doi:10.1109/TEVC.2019.2909744.

[2] J. J. Liang, B. Y. Qu, D. W. Gong, C. T. Yue, Problem definitions and evaluation criteria for the CEC 2019 special session on multimodal multiobjective optimization, Technical Report, Computational Intelligence Laboratory, Zhengzhou University (2019).

[3] C. Yue, B. Qu, J. Liang, A multiobjective particle swarm optimizer using ring topology for solving multimodal multiobjective problems, IEEE Transactions on Evolutionary Computation 22 (5) (2018) 805–817. doi:10.1109/TEVC.2017.2754271.

[4] S. Bandyopadhyay, A. Mukherjee, An algorithm for many-objective optimization with reduced objective computations: A study in differential evolution, IEEE Transactions on Evolutionary Computation 19 (3) (2015) 400–413.

[5] K. Deb, A. Pratap, S. Agarwal, T. Meyarivan, A fast and elitist multiobjective genetic algorithm: NSGA-II, IEEE Transactions on Evolutionary Computation 6 (2) (2002) 182–197. doi:10.1109/4235.996017.

[6] Y. Tian, X. Zhang, R. Cheng, Y. Jin, A multi-objective evolutionary algorithm based on an enhanced inverted generational distance metric, in: 2016 IEEE Congress on Evolutionary Computation (CEC), 2016, pp. 5222–5229. doi:10.1109/CEC.2016.7748352.

[7] P. A. N. Bosman, D. Thierens, The balance between proximity and diversity in multiobjective evolutionary algorithms, IEEE Transactions on Evolutionary Computation 7 (2) (2003) 174–188.

[8] K. Li, K. Deb, Q. Zhang, S. Kwong, An evolutionary many-objective optimization algorithm based on dominance and decomposition, IEEE Transactions on Evolutionary Computation 19 (5) (2015) 694–716.
[9] J. Bader, E. Zitzler, HypE: An algorithm for fast hypervolume-based many-objective optimization, Evolutionary computation 19 (1) (2011) 45–76.
[10] R. Sengupta, M. Pal, S. Saha, S. Bandyopadhyay, Population dynamics indicators for evolutionary many-objective optimization, in: Progress in Advanced Computing and Intelligent Engineering, Springer, 2019, pp. 261–271.
[11] Y. Tian, R. Cheng, X. Zhang, F. Cheng, Y. Jin, An indicator based multi-objective evolutionary algorithm with reference point adaptation for better versatility, IEEE Transactions on Evolutionary Computation (2017).
[12] J. J. Liang, C. T. Yue, B. Y. Qu, Multimodal multi-objective optimization: A preliminary study, in: 2016 IEEE Congress on Evolutionary Computation (CEC), IEEE, 2016, pp. 2454–2461.
[13] R. Langone, O. Mauricio Agudelo, B. De Moor, J. A. Suykens, Incremental kernel spectral clustering for online learning of non-stationary data, Neurocomputing 139 (2014) 246 – 260. doi:https://doi.org/10.1016/j.neucom.2014.02.036.
URL http://www.sciencedirect.com/science/article/pii/S0925231214004433